Chapter 6: Structural Elucidation of a β-amino-γ-linked Cyclic Polyamide-DNA Complex and RNA Binding Studies

Abstract

Chemical control of dysregulated gene expression poses a significant challenge at the frontier of chemical biology. Py-Im polyamides are a class of small molecules that can be programmed to bind a broad repertoire of DNA sequences, disrupt transcription factor-DNA interfaces, and modulate gene expression pathways in cell culture experiments. Detailed structural information thus far has been limited to moderate resolution X-ray structures of unlinked 2:1 binding polyamides and NMR NOESY-restrained molecular dynamics models, with atomic resolution X-ray structures remaining elusive. Structural elucidation of polyamide-DNA complexes is fundamental to understanding the recognition properties at the molecular level and this chapter reports a high resolution (0.95 Å) X-ray crystal structure of a cyclic Py-Im polyamide bound to the central six base pairs of the sequence d(5'-CCAGTACTGG-3')$_2$, revealing the hydrophobic, electrostatic, and shape selective recognition interactions responsible for DNA binding. Additionally, a structural basis for the allosteric modulation of transcription-factor DNA interfaces with β-amino turn linked cyclic polyamides is reported and a combination of biophysical, structural, and modeling studies are presented which explain the inability of polyamides to bind double helical A-form RNA.

6.1 Introduction

Pyrrole-imidazole polyamides are a class of small molecules that bind the minor groove of DNA sequence specifically.[1,2] Encoded by side-by-side arrangements of *N*-methylpyrrole (Py) and *N*-methylimidazole (Im) carboxamide monomers, Im/Py pairs distinguish G•C from C•G base pairs, whereas Py/Py pairs are degenerate for T•A and A•T.[3-6] Polyamides have been shown to bind a broad repertoire of DNA sequences,[7] permeate cell membranes and traffic to the nucleus,[8-15] access chromatin, [16,17]and disrupt protein-DNA interactions.[2] Polyamide inhibition of transcription factor-DNA binding of HIF-1α,[18,19,20] androgen receptor (AR),[21] and AP-1[22,23] has been exploited for controlling expression of medically relevant genes such as VEGF, PSA, TGF-β1 and LOX-1 in cell culture experiments. X-ray crystallography has provided structures of unlinked 2:1 binding polyamides to a resolution of 2.00 Å, providing valuable insight into the polyamide-DNA molecular recognition process.[5,6,24] Structural studies of hairpin polyamides bound to the nucleosome core particle have also provided structural proof that polyamides can bind biologically relevant higher order structure, however a combination of resolution limits and high B-factors prevented a detailed picture of the polyamide-DNA interactions beyond confirmation of the binding location.[16,25] Much insight has been gleaned from NMR studies where NOESY-restrained molecular dynamics models have provided structures of 1:1 and 6-ring cyclic polyamides.[26,27] Despite these successes, atomic resolution X-ray structures of this important class of compounds and in general minor groove binders have remained elusive.

The ability of DNA to undergo bending, twisting, and stretching motions as well as the long-range propagation (allosteric effect) of these perturbations coupled with DNA recognition by proteins and small molecules can have profound influences over important processes such as gene transcription and modulation of eukaryotic gene networks.[28-32] Allosteric communication along and through the DNA helix has been the subject of intense study and forms the basis for cooperative interactions among transcription factor regulatory networks such as the interferon-β enhanceosome, where transcription factor binding induced DNA conformational changes led to cooperative enhancer occupancy. This potential for short and long range allosteric control over the transcriptional machinery provides a powerful concept for the design of small molecules that can bind to topographically distinct locations on DNA with the possibility of modulating transcription factor-DNA binding by allosteric perturbation of the DNA structure.[30,31] Recent studies (Chapter 3) of cyclic polyamide **1** and analogous hairpin polyamides revealed they possessed high DNA binding affinities and could regulate endogenous androgen receptor-activated gene expression (prostate

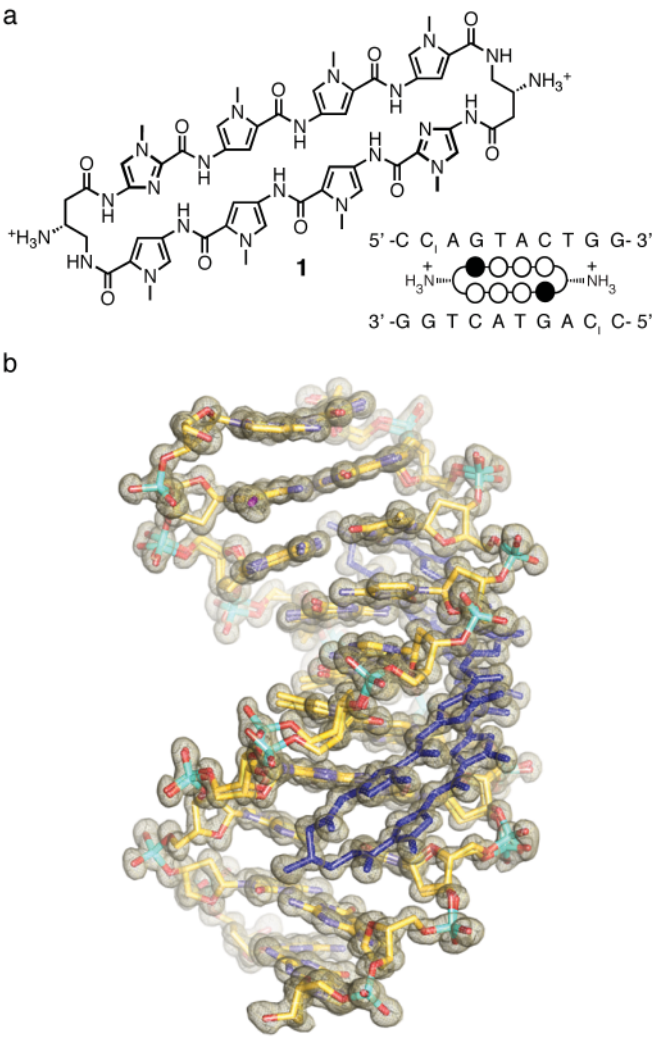

Figure 6.1 Structure of cyclic polyamide **1** presented with its ball-and-stick model superimposed over the binding site on the dsDNA oligonucleotide sequence used for crystallization. Closed circles designate *N*-methylimidazole, open circles designate *N*-methylpyrrole, and half open circles substituted with ammoniums designate β-amino substituted γ-turn unit. b. Electron density map contoured at the 1.0 σ level for the X-ray crystal structure of cyclic polyamide **1** complexed to ds-DNA (0.95 Å resolution).

specific antigen) in cell culture, from which we infer cell permeability. Additionally, In vitro ADMET studies of cycle **1** and hairpin polyamides revealed favorable drug-like properties for both classes of compounds and excellent metabolic stability.

Reported, is the atomic resolution structure (0.95 Å resolution) of an 8-ring cyclic polyamide in complex with double helical DNA. The cyclic polyamide **1** is comprised of two antiparallel ImPyPyPy strands capped by (*R*)-β-amino-γ turn units. Polyamide **1**, which codes for the sequence 5'-WGWWCW-3' was cocrystallized with the palindromic DNA oligonucleotide sequence 5'-CC$_I$AGTACTGG-3' 10 base pairs in length (Fig. 6.1). We observe significant allosteric structural perturbations of the DNA helix induced upon binding of substituted GABA (γ-aminobutyric acid) turn-linked polyamides in the DNA minor groove. In addition to amide and imidazole recognition with the DNA minor groove floor, a detailed view of the β-amino-γ-turn conformation and hydration reveals a network of well-ordered water-mediated interactions between the polyamide and DNA. Significantly, we find that a conformational inversion occurs at the turn position upon moving the amino substituent from the α to β positions of the GABA turn. The allosteric modulation of the DNA structure induced by polyamide binding is also shown and a structural basis for the inability of polyamides to bind A-form

Table 6.1 Data collection and refinement statistics.

Data collection		
	Space group	$P4_12_12$
	Cell dimensions	
	a, b, and c, Å	39.83
		39.83
		84.57
	α, β, and γ, °	90
		90
		90
	Wavelength	0.82654
	Resolution, Å	23.44 - 0.95
	R_{merge}*	9.0 (52.7)
	$I/\sigma I$*	13.9 (2.3)
	Completeness, %*	97.7 (99.6)
	Redundancy	7.4
Refinement		
	Resolution, Å	23.44 - 0.95
	No. of reflections	39,782
	R_{work}/R_{free}‡	11.2 / 12.4
	No. of atoms	
	DNA	445
	Polyamide	86
	Calcium	4
	Water	239
	B factors	
	DNA	7.2
	Polyamide	6.7
	Calcium	13.2
	Water	23.1

*Highest-resolution shell is shown in parentheses.
‡Free *R* calculated against 5% of the reflections randomly removed.

RNA is presented with UV-melting temperature data.

6.2 Overall Structure

The structure of cyclic polyamide **1** in complex with d(5'-$CC_IAGTACTGG)_2$ was solved by direct methods to 0.95 Å resolution with synchrotron radiation (Fig. 6.1). One cyclic polyamide bound to a single DNA duplex is present in the asymmetric unit of the crystal in the $P4_12_12$ space group. The final structure was refined anisotropic and unrestrained to an *R*-factor of 11.2% and an R_{free} of 12.4% (Table 6.1). The average B-factor for the polyamide was 6.7 $Å^2$ and 7.2 $Å^2$ for DNA. The asymmetric unit contains one full polyamide-complexed DNA double helix. In the DNA complex, the aromatic amino acids are bound with an N- to C-orientation of each ImPyPyPy strand of the cycle adjacent to the 5' to 3' direction of the DNA. The conformational constraints imposed by the turn unit result in ring placement that is ring-over-ring as opposed to ring-over-amide. Greater than 40% of the polyamide surface area is buried leaving only the top of the methyl groups on the heterocycles, the amide carbonyl oxygens, and the chiral β-ammonium turn solvent exposed. Alternate conformations are observed for 7 of the 18 nucleotides of the DNA duplex. The cyclic pyrrole-imidazole polyamide **1** was co-crystallized with the palindromic DNA oligonucleotide sequence shown in Figure 6.1. The polyamide selectively binds to the sequence, 5'-WGTACW-3', and previous studies have demonstrated that the equilibrium binding constants are sub-nanomolar and outside the measurement range of DNase I footprinting methods (see Chapter 3).

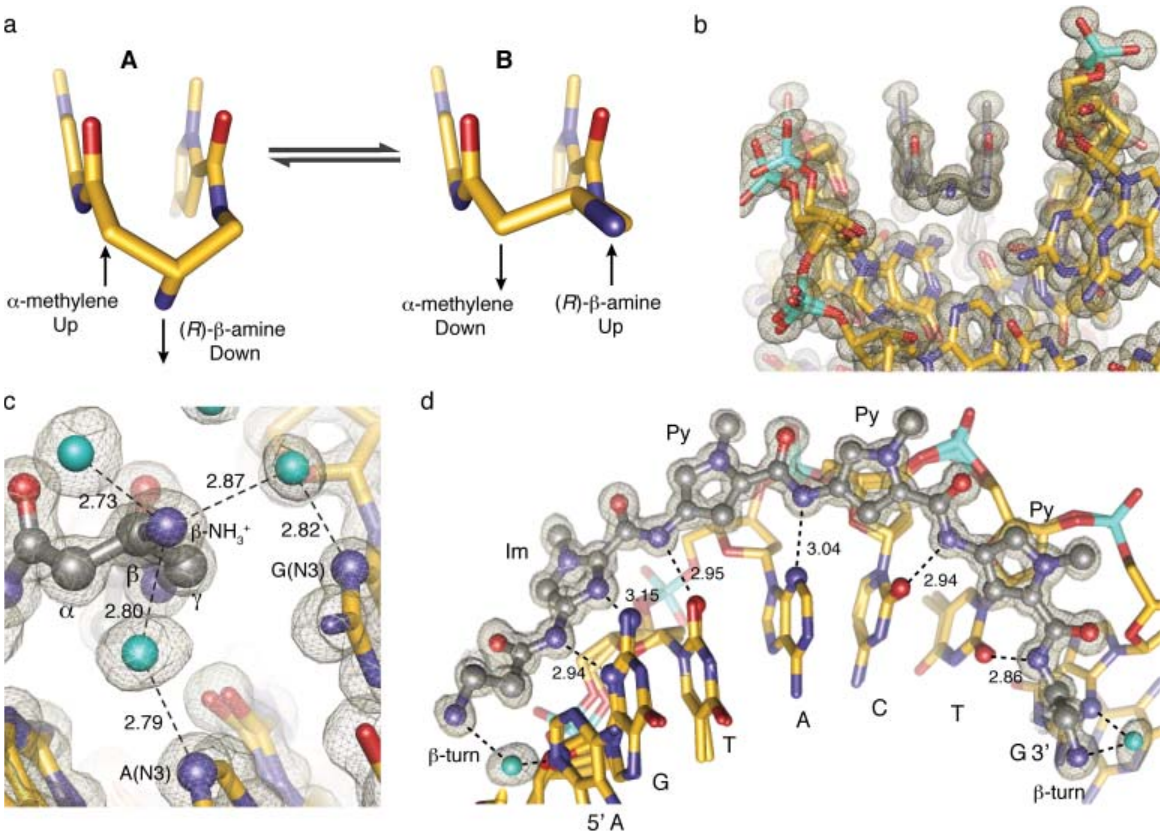

Figure 6.2 Molecular recognition details from the X-ray structure of cyclic polyamide **1**. a. Conformation of the β-amino substituted GABA turn linkage. Conformation A (left) is the conformation observed in the previously determined α-amino turn X-ray crystal structure. Conformation B (right) shows the preferred conformation for the β-amino turn determined by X-ray crystallography in this report. The β-methine conformational preference is puckered up and away from the DNA minor-groove floor, aligning the β-ammonium along the groove floor. b. Structural view looking down the DNA minor groove showing the bound cyclic polyamide with electron density contoured at the 1.0 σ level. c. Geometry of the alpha-amino turn interacting with the adenine and guanine base pairs in the floor of the DNA minor groove through water-mediated hydrogen bonds. d. Isolated view of one half of the polyamide (split along a plane through the long axis of the polyamide and the DNA helical axis) showing hydrogen bond distances made to the DNA minor groove floor. Hydrogen bonding interactions of the DNA-polyamide complex with electron density contoured at the 1.0 σ level. (Im = imidazole and Py = pyrrole)

6.3 Overall structure of DNA-polyamide complex

The cyclic pyrrole-imidazole polyamide is bound in an antiparallel head-to-tail turn-linked fashion with the N- to C-terminal orientation of each PyPyPyIm strand of the polyamide directly adjacent to a DNA strand oriented in a 5' to 3' direction. Figure 6.1 shows the overall structure of the complex with the electron density map contoured to the 1.0 σ level. Figure 6.2b shows a view of the complex looking directly down the minor groove at the polyamide turn linkage. From this view it can be seen that significant stabilization of the complex is derived from van der Waals

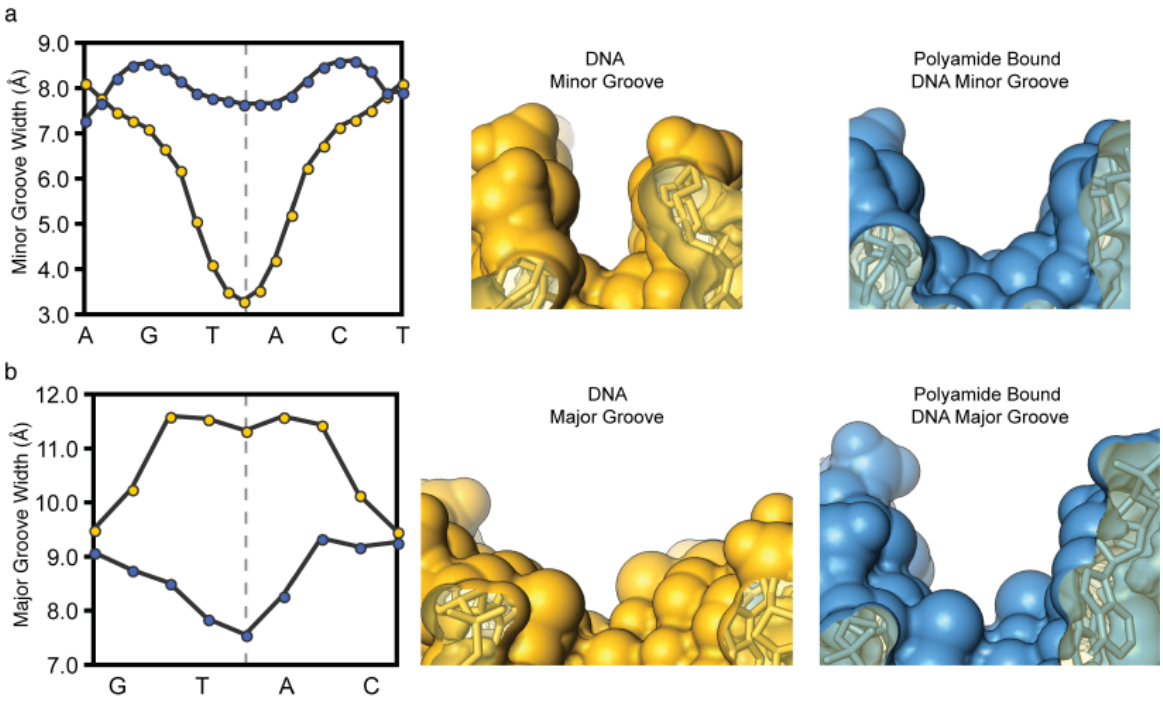

Figure 6.3 DNA minor and major groove dimensions in the absence and presence of polyamide. Native DNA structure d(5'-CCAGTACTGG-3')$_2$ solved by Rees and coworkers (PDB: 1d8g, 0.74 Å resolution). a. Comparison of the minor groove width for DNA in the absence of polyamide (yellow curve and structure) and in the presence of bound polyamide (blue curve and structure). b. Comparison of the major groove width for DNA in the absence of polyamide (yellow curve and structure) and in the presence of bound polyamide (blue curve and structure). note: polyamide has been removed from the blue complex for clarity.

interactions between the outside face of the pyrrole-imidazole heterocyclic strands and the walls of the minor groove, which form a deep binding pocket for the polyamide. Greater than 40% of the polyamide surface area is buried and not solvent exposed, leaving only the top of the methyl groups of the heterocycles, the amide carbonyl oxygens, and the chiral β-amino turn linkage solvated. The turn linkage adds a conformational constraint to the ends of the polyamides preventing the heterocycle strands from slipping past each other as observed in the slipped orientations found in some 2:1 binders such as distamycin.

6.4 Turn conformation

The β-methine conformational preference is puckered up and away from the DNA minor-groove floor, aligning the β-ammonium along the groove. Conformation A (left) is the conformation observed in the previously determined α-amino turn X-ray crystal structure. Conformation B (right) shows the preferred conformation for the β-amino turn determined by

X-ray crystallography in this report. The hydration pattern around the turn is highly conserved at both ends of the structure and there are two water-mediated hydrogen bonds within 2.79 - 2.87 Å from the ammonium to the DNA minor-groove floor (Fig. 6.2c). The amide NH's and imidazole lone-pairs form a continuous series of direct hydrogen bonds to the floor of the DNA minor-groove, while the imidazoles impart specificity for the exocyclic amine of guanine through relief of steric interaction and a G(N2-hydrogen)-Im (lone pair) hydrogen bond (Fig. 6.2c-d). The amides linking the aromatic rings and the turns contribute hydrogen bonds to the purine N3 and pyrimidine O2 lone pairs where they all are within hydrogen bonding distance of a single DNA base. In total there are 10 direct amide hydrogen bonds (2.86–3.08 Å), 2 direct imidazole hydrogen bonds (3.15 and 3.16 Å), and 4 (*R*)-β-ammonium turn water-mediated hydrogen bonds (two per turn, average distance from amine to water = 2.79 Å–2.87 Å) to the floor of the DNA minor groove with at least one interaction for all 12 DNA base-pairs in the 6 bp binding site. There are a total of 16 hydrogen bond interactions between the cyclic polyamide and the floor of the DNA minor-groove, utilizing every hydrogen-bond donor and acceptor of the ligand (Fig. 6.2).

6.5 Allosteric Perturbations

Polyamide binding induces large structural changes in DNA and Figure 6.3 shows a

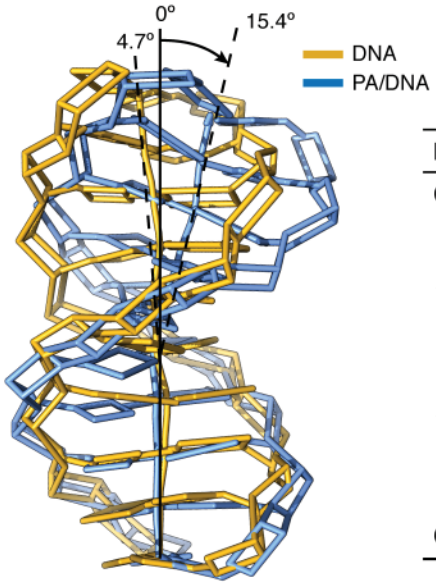

	Roll, °		Twist, °	
bp step	DNA	PA/DNA	DNA	PA/DNA
CC/GG	9.03	7.70	28.26	33.68
CA/TG	-7.95	8.79	50.50	30.23
AG/CT	9.87	11.19	21.04	35.16
GT/AC	-0.74	2.85	35.80	32.13
TA/TA	3.26	7.23	48.48	35.93
AC/GT	-0.74	2.47	35.80	32.04
CT/AG	9.89	10.59	21.04	35.32
TG/CA	-7.96	9.57	50.49	29.68
GG/CC	9.03	3.58	28.26	32.64

Figure 6.4 Allosteric distortion upon polyamide binding. (left) DNA bending is observed for polyamide-bound DNA (blue structure) versus unbound-DNA (yellow structure). (right) Helical parameters for DNA in the absence and presence of polyamide showing an increase in positive roll and significant changes in twist angles upon polyamide binding. (Polyamide has been removed from the blue complex for clarity)

Table 6.2 Buckle and opening values.

	Buckle, °		Opening, °	
bp step	DNA	PA/DNA	DNA	PA/DNA
C•G	-6.41	-10.59	0.99	0.68
C•G	-0.43	-7.08	-1.15	1.71
A•T	-1.63	6.15	1.35	3.84
G•C	10.75	-2.23	1.26	-0.78
T•A	13.15	0.37	-0.27	-4.87
A•T	-13.15	1.17	-0.27	-4.88
C•G	-10.74	2.39	1.27	-1.10
T•A	1.63	-2.93	1.34	3.78
G•C	0.44	16.58	-1.13	0.87
G•C	6.42	23.00	1.00	-0.15

slice through the short axis of the DNA helix showing the minor and major groove geometry at the center of the polyamide binding site for uncomplexed and complexed DNA. Figure 6.3 reveals a >4 Å widening of the DNA minor groove upon polyamide binding and a compression of the major groove by more than 4 Å. Additionally, Figure 6.3 shows a major perturbation in the major groove depth upon polyamide binding converting the wide shallow surface of the major groove from a functionally exposed protein recognition domain to a narrow deep cleft less likely to accomodate the width of a standard protein alpha-helical domain or beta-sheet from a transcription factor. Figure 6.4 shows the polyamide induced bending of the DNA helix. The helix is bent toward the major groove by >15º resulting in major groove compression. The base-pair step parameters in Figure 6.4 show a large positive roll throughout the polyamide binding site which contributes to the significant bend in the DNA helix. Additionally, polyamide binding induces a more uniform helical twist resulting in less variability as the base-pair step changes. The helical twist values for polyamide bound DNA range from 29.68-35.93º. Values for the helical twist are highly sequence dependent in native DNA and range from 21.04 to 50.50º depending on step sequence. Major perturbations in the DNA base pair buckle and opening are also observed upon polyamide binding. At the central 4 base pairs of the binding site the buckle is significantly reduced upon binding and the base pairs are opened toward the DNA major groove with the largest variations occuring at the central AT base pairs. [Note: For a full set of helical parameters and definitions see Figures 6.6, 6.7, and 6.8.]

6.6 Solvation

The structure has a cell volume of 134,162 $Å^3$ and a Matthews Coefficient of 2.24 with a solvent content of 51%. There are 130 out of 239 water molecules within 3.0 Å of the polyamide-DNA complex and 76 of the 130 water molecules localized around the DNA phosphates. The solvent exposed surface of the polyamide is hydrated by 22 of the 130 waters found within 3.0 Å of the complex.

Table 6.3 Polyamide-DNA and Polyamide-RNA melting temperatures.

		dsDNA sequence		dsRNA sequence	
		5′–CC**AGTACT**GG–3′ 3′–GG**TCATGA**CC–5′		5′–CC**AGUACU**GG–3′ 3′–GG**UCAUGA**CC–5′	
Polyamides		T_m / °C	ΔT_m / °C	T_m / °C	ΔT_m / °C
—		46.1 (±0.8)	—	60.4 (±0.6)	—
^+H_3N···  ···NH_3^+	(**1**)	82.8 (±0.6)	36.6 (±1.0)	59.9 (±0.8)	-0.5 (±1.0)
IPA–  ···NH_3^+	(**2**)	72.3 (±0.5)	26.2 (±1.0)	60.7 (±0.5)	0.3 (±0.8)
Dp–  –Dp	(**3**)	52.8 (±0.4)	6.6 (±0.9)	59.7 (±0.3)	-0.6 (±0.7)

These waters cluster and form bridges across the carbonyl oxygens of adjacent amides linking ring pairs, resulting in stripes of well ordered water across the polyamide surface. Additionally, 6 waters hydrate the polyamide ammonium turns (3 at each turn) with 4 of the 6 anchoring the polyamide to the floor of the DNA minor groove through bridging hydrogen bonds.

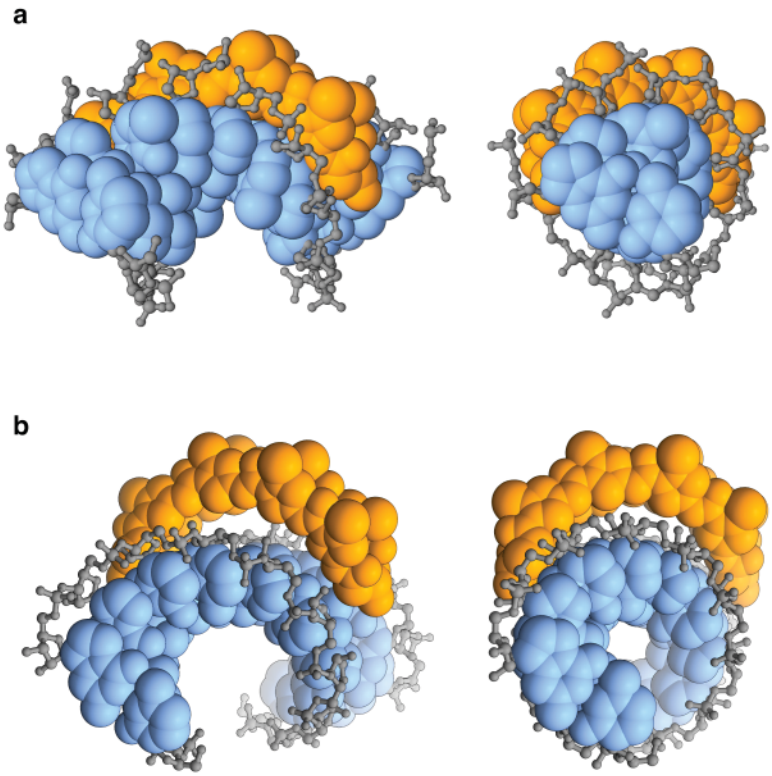

Figure 6.5 a. Crystal structure of DNA-polyamide complex showing shape complementary and favorable hydrophobic interactions with the sugar-phosphate backbone. b. Coordinates of the cyclic polyamide docked within van der Waals radius of the putative binding site on a model of ideal A-form double helical RNA.

6.7 RNA Binding Studies

The minor groove binding of polyamides to B-form DNA has been extensively studied, however the ability of polyamides to bind double helical RNA has received little attention. There are two major differences in helical RNA versus DNA. First, thyamine (T) is replaced by uracil (U) presenting the addition of a 5' methyl group to the major groove of the helix. However, the hydrogen

bonding functionality of the minor groove remains identical to that of B-form DNA. The second and most important difference is the addition of a 2'–OH on the sugar resulting in ribose as opposed to deoxyribose for DNA. This extra hydroxyl has a profound effect on the overall helical RNA structure and rigidity primarily due to the enforcement of a C3'–endo ribose sugar pucker. This pucker forces the RNA helix into an A or A'-form conformation due to the steric incompatibility of the 2'–OH with a DNA B-form conformation, which prefers a C2'–endo sugar conformation. The conformational rigidity leads to less sequence dependent microstructure than DNA and a dramatically different minor and major groove geometry. Additionally, the DNA helix has been shown to be highly conformationally mobile in contrast to the RNA helix. The structure of A-form RNA has an 11-fold helix with a narrow, deep major groove and shallow, wide minor groove in stark contrast to B-form DNA. The base pairs of A-form RNA are inclined and drastically displaced from the helix axis causing an overall expansion of the helix width, which in turn leads to a dramatically shallow curvature of the minor groove floor. The criteria required for polyamide binding and, in general, small molecule binding relies on the minimization of water exposed hydrophobic surfaces, the complementary pairing of buried hydrogen bond donors and acceptors, the maximization of van der Waals interactions, the solvation or neutralization of all charges, and the maximization of attractive and minimization of repulsive interactions. Our results show that the polyamides in this study provide a large thermal stabilization to DNA as opposed to RNA, which does not have an increased melting temperature for any of the compounds studied. The thermal stabilization for the DNA duplex ranges from 4 ºC for the unlinked polyamide (2:1 complex at saturating concentrations) to 23 ºC for the cyclic polyamide.

6.8 Conclusion

The crystal structure presented highlights the molecular recognition of β-amino turn-linked polyamides in the minor-groove of DNA and provides insight into the allosteric modulation of B-form DNA by Py-Im polyamides. The DNA structural distortion induced upon polyamide minor-groove binding provides an allosteric model for disrupting DNA:transcription factor interfaces in the promoters of selected genes. The ability of DNA to undergo short and long-range allosteric effects coupled with DNA binding by proteins can have influence over important processes such as modulation of eukaryotic gene networks. The potential for allosteric control over the transcriptional machinery provides a powerful concept for the design of small molecules that can bind to distinct locations on DNA with the possibility of modulating transcription factor activity. The RNA binding

studies demonstrate that this class of Py-Im polyamides are completely selective for binding dsDNA over dsRNA.

6.9 Experimental

6.9.1 Synthesis

Polyamides **1**–**3** were synthesized by standard solution-phase synthesis methods presented in Chapter 2 and 3 of this thesis. Synthetic deoxyoligonucleotides were purchased HPLC purified from Trilink Biotechnologies and desalted using a 5 gram sep-pak C18 cartridge (Waters) followed by lyophilization to dryness.

6.9.2 Oligonucleotide purification and Crystallization

Oligonucleotides were purchased HPLC purified from Trilink Biotechnologies (San Diego, CA). Prior to use the oligonucleotides were de-salted using a 5 gram sep-pak C18 cartridge (Waters) and lyophilized to dryness.

Single stranded DNA was quantitated by UV-Vis spectroscopy and incubated with a 2:1 ratio of DNA to polyamide prior to crystallization. Crystals were obtained from a solution of 0.6 mM duplex DNA, 0.75 mM polyamide, 24% 2-methyl-2,4-pentanediol (MPD), 35 mM calcium acetate, 10 mM Tris pH 7.5 equilibrated in sitting drops against a reservoir of 35% MPD at 4ºC and crystals were flash cooled at 100 K prior to data collection. DNA crystals grew in space group $P4_12_12$ with unit cell dimensions a = 39.8270Å, b = 39.8270Å, c = 84.5718Å, α = 90.00º, β = 90.00º, γ = 90.00º.

6.9.3 Data collection, Structure determination, and refinement

Polyamide-DNA crystals grew in space group $P4_12_12$ with unit cell dimensions a = 39.8270Å, b = 39.8270Å, c = 84.5718Å, α = 90.00º, β = 90.00º, γ = 90.00º, and one polyamide-duplex DNA complex in the asymmetric unit. This data set was collected at Stanford Synchrotron Radiation Laboratory (SSRL) beamline 12-2 with a MAR Research imaging plate plate detector at wavelength 0.97 Å.

Data was processed with Mosflm[33] and scaled with the CCP4[34] program suite. Solution of both structures was obtained using SHELXD[35,36] direct methods. All atoms were visible in initial maps from direct methods solution. Refinement was performed using Refmac[37] and model building using Coot.[38]

6.9.4 Structure Analysis

DNA helical parameters were calculated using the program Curves[39] and 3DNA.[40] Figures were prepared and measurements made using UCSF Chimera.[41]

6.10 Notes and References

1. Dervan, P. B. Molecular recognition of DNA by small molecules. *Bioorg. Med. Chem.* **2001**, *9*, 2215-2235.

2. Dervan, P. B., and Edelson, B. S. Recognition of the DNA minor groove by pyrrole-imidazole polyamides *Curr. Opin. Struct. Biol.* **2003**, *13*, 284-299.

3. Trauger, J. W., Baird, E. E., and Dervan, P. B. Recognition of DNA by designed ligands at subnanomolar concentrations. *Nature*. **1996**, *382*, 559-561.

4. White, S., Szewczyk, J. W., Turner, J. M., Baird, E. E., and Dervan, P. B. Recognition of the four Watson-Crick base pairs in the DNA minor groove by synthetic ligands. *Nature*. **1998,** *391*, 468-470.

5. Kielkopf, C. L., Baird, E. E., Dervan, P. B., and Rees, D. C. Structural basis for G•C recognition in the DNA minor groove. *Nat. Struct. Biol.* **1998**, *5*, 104-109.

6. Kielkopf, C. L., White, S., Szewczyk, J. W., Turner, J. M., Baird, E. E., Dervan, P. B., and Rees, D. C. A structural basis for recognition of A•T and T•A base pairs in the minor groove of B-DNA. *Science*. **1998**, *282*, 111-115.

7. Hsu, C. F., Phillips, J. W., Trauger, J. W., Farkas, M. E., Belitsky, J. M., Heckel, A., Olenyuk, B. Z., Puckett, J. W., Wang, C. C. C., and Dervan, P. B. Completion of a programmable DNA-binding small molecule library. *Tetrahedron*. **2007**, *63*, 6146-6151.

8. Belitsky, J. M., Leslie, S. J., Arora, P. S., Beerman, T. A., and Dervan, P. B. Cellular uptake of *N*-methylpyrrole/*N*-methylimidazole polyamide-dye conjugates. *Bioorg. Med. Chem.* **2002**, *10*, 3313-3318.

9. Crowley, K. S., Phillion, D. P., Woodard, S. S., Scheitzer, B. A., Singh, M., Shabany, H., Burnette, B., Hippenmeyer, P., Heitmeier, M., and Bashkin, J. K. Controlling the intracellular localization of fluorescent polyamide analogues in cultured cells. *Bioorg. Med. Chem. Lett.* **2003**, *13*, 1565-1570.

10. Best, T. P., Edelson, B. S., Nickols, N. G., and Dervan, P. B. Nuclear localization of pyrrole-imidazole polyamide-fluorescein conjugates in cell culture. *Proc. Natl. Acad. Sci. U. S. A.* **2003**, *100*, 12063-12068.

11. Edelson, B. S., Best, T. P., Olenyuk, B., Nickols, N. G., Doss, R. M., Foister, S., Heckel, A., and Dervan, P. B. Influence of structural variation on nuclear localization of DNA-binding polyamide-fluorophore conjugates. *Nucleic. Acids. Res.* **2004**, *32*, 2802-2818.

12. Xiao, X., Yu, P., Lim, H. S., Sikder, D., and Kodadek, T. A cell-permeable synthetic transcription factor mimic. *Angew. Chem. Int. Ed. Engl.* **2007**, *46*, 2865-2868.

13. Nickols, N. G., Jacobs, C. S., Farkas, M. E., and Dervan, P. B. Improved nuclear localization of DNA-binding polyamides. *Nucleic. Acids. Res.* **2007**, *35*, 363-370.

14. Dose, C., Farkas, M. E., Chenoweth, D. M., and Dervan, P. B. Next generation hairpin polyamides with (R)-3,4-diaminobutyric acid turn unit. *J. Am. Chem. Soc.* **2008**, *130*, 6859-6866.

15. Hsu, C. F., and Dervan, P. B. Quantitating the concentration of Py-Im polyamide-fluorescein conjugates in live cells. *Bioorg. Med. Chem. Lett.* **2008**, *18*, 5851-5855.

16. Edayathumangalam, R. S., Weyermann, P., Gottesfeld, J. M., Dervan, P. B., and Luger, K. Molecular recognition of the nucleosomal "supergroove". *Proc. Natl. Acad. Sci. U. S. A.* **2004**, *101*, 6864-6869.

17. Dudouet, B., Burnett, R., Dickinson, L. A., Wood, M. R., Melander, C., Belitsky, J. M., Edelson, B., Wurtz, N., Briehn, C., Dervan, P. B., and Gottesfeld, J. M. Accessibility of nuclear chromatin by DNA binding polyamides. *Chem. Biol.* **2003**, *10*, 859-867.

18. Olenyuk, B. Z., Zhang, G. J., Klco, J. M., Nickols, N. G., Kaelin, Jr., W. G., and Dervan, P. B. Inhibition of vascular endothelial growth factor with a sequence-specific hypoxia response element antagonist. *Proc. Natl. Acad. Sci. U. S. A.* **2004**, *101*, 16768-16773.

19. Kageyama, Y., Sugiyama, H., Ayame, H., Iwai, A., Fujii, Y., Huang, L. E., Kizaka-Kondoh, S., Hiraoka, M., and Kihara, K. Suppression of VEGF transcription in renal cell carcinoma cells by pyrrole-imidazole hairpin polyamides targeting the hypoxia responsive element. *Acta. Oncol.* **2006**, *45*, 317-324.

20. Nickols, N. G., Jacobs, C. S., Farkas, M. E., and Dervan, P. B. Modulating hypoxia-inducible transcription by disrupting the HIF-1-DNA interface. *ACS. Chem. Biol.* **2007**, *2*, 561-571.

21. Nickols, N. G., and Dervan, P. B. Suppression of androgen receptor-mediated gene expression by a sequence-specific DNA-binding polyamide. *Proc. Natl. Acad. Sci. U. S. A.* **2007**, *104*, 10418-10423.

22. Matsuda, H., Fukuda, N., Ueno, T., Tahira, Y., Ayame, H., Zhang, W., Bando, T., Sugiyama, H., Saito, S., Matsumoto, K., and others, O. Development of gene silencing pyrrole-imidazole polyamide targeting the TGF-beta1 promoter for treatment of progressive renal diseases. *J. Am. Soc. Nephrology.* **2006**, *17*, 422-432.

23. Yao, E. H., Fukuda, N., Ueno, T., Matsuda, H., Matsumoto, K., Nagase, H., Matsumoto, Y., Takasaka, A., Serie, K., Sugiyama, H., and Sawamura, T. Novel gene silencer pyrrole-imidazole polyamide targeting lectin-like oxidized low-density lipoprotein receptor-1 attenuates restenosis of the artery after injury. *Hypertension.* **2008**, *52*, 86-92.

24. Kielkopf, C. L., Bremer, R. E., White, S., Szewczyk, J. W., Turner, J. M., Baird, E. E., Dervan, P. B., and Rees, D. C. Structural effects of DNA sequence on TA recognition by hydroxypyrrole/pyrrole pairs in the minor groove. *J. Mol. Biol.* **2000**, *295*, 557-567.

25. Suto, R. K., Edayathumangalam, R. S., White, C. L., Melander, C., Gottesfeld, J. M., Dervan, P. B., and Luger, K. Crystal structures of nucleosome core particles in complex with minor groove DNA-binding ligands. *J. Mol. Biol.* **2003**, *326*, 371-380.

26. Urbach, A. R., Love, J. J., Ross, S. A., and Dervan, P. B. Structure of a beta-alanine-linked polyamide bound to a full helical turn of purine tract DNA in the 1:1 motif. *J. Mol. Biol.* **2002**, *320*, 55-71.

27. Zhang, Q., Dwyer, T. J., Tsui, V., Case, D. A., Cho, J., Dervan, P. B., and Wemmer, D. E. NMR structure of a cyclic polyamide-DNA complex. *J. Am. Chem. Soc.* **2004**, *126*, 7958-7966.

28. Crothers, D. M., and Fried, M. Transmission of long-range effects in DNA. *Cold. Spring. Harb.*

Symp. Quant. Biol. **1983**, *47*, 263-269.

29. Lavelle, C. DNA torsional stress propagates through chromatin fiber and participates in transcriptional regulation. *Nat. Struct. Mol. Biol.* **2008**, *15*, 146-154.

30. Mathew-Fenn, R. S., Das, R., and Harbury, P. A. Remeasuring the double helix. *Science* **2008**, *322*, 446-449.

31. Nguyen-Hackley, D. H., Ramm, E., Taylor, C. M., Joung, J. K., Dervan, P. B., and Pabo, C. O. Allosteric inhibition of zinc-finger binding in the major groove of DNA by minor-groove binding ligands. *Biochemistry.* **2004**, *43*, 3880-3890.

32. Moretti, R., Donato, L. J., Brezinski, M. L., Stafford, R. L., Hoff, H., Thorson, J. S., Dervan, P. B., and Ansari, A. Z. Targeted chemical wedges reveal the role of allosteric DNA modulation in protein-DNA assembly. *ACS. Chem. Biol.* **2008**, *3*, 220-229.

33. Leslie, A. G. W. Recent changes to the MOSFLM package for processing film and image plate data. *Acta. Crystallogr. D. Biol. Crystallogr.* **1992**, *26*.

34. Collaborative Computational Project, No. 4. The CCP4 suite: programs for protein crystallography. *Acta. Crystallogr.* **1994**, *50*, 760-763.

35. Schneider, T. R., and Sheldrick, G. M. Substructure solution with SHELXD. *Acta. Crystallogr. D. Biol. Crystallogr.* **2002**, *58*, 1772-1779.

36. Sheldrick, G.M. A short history of SHELX. *Acta Crystallogr. A* **64**, 112-122 (2008).

37. Murshudov, G. N., Vagin, A. A., and Dodson, E. J. Refinement of macromolecular structures by the maximum-likelihood method. *Acta. Crystallogr. D. Biol. Crystallogr.* **1997**, *53*, 240-255.

38. Emsley, P., and Cowtan, K. Coot: model-building tools for molecular graphics. *Acta. Crystallogr. D. Biol. Crystallogr.* **2004**, *60*, 2126-2132.

39. Lavery, R., and Sklenar, H. Curves 5.2: Helical analysis of irregular nucleic acids. *Biochimie. Theorique,. CNRS. URA.* **1997**, *77*.

40. Lu, X. J., Olson, W. K. 3DNA: a software package for the analysis, rebuilding and visualization of three-dimensional nucleic acid structures. *Nucleic Acids. Res.*, **31**, 5108-5121 (2003).

41. Pettersen, E. F., Goddard, T. D., Huang, C. C., Couch, G. S., Greenblatt, D. M., Meng, E. C., and Ferrin, T. E. UCSF Chimera--a visualization system for exploratory research and analysis. *J. Comput. Chem.* **2004**, *25*, 1605-1612.

6.11 Supplemental Information

Local base-pair step parameters

Parameter*	CC/GG	CA/TG	AG/CT	GT/AC	TA/TA	AC/GT	CT/AG	TG/CA	GG/CC
Shift, Å									
DNA	-0.58	0.23	0.58	-0.73	0.00	0.73	-0.58	-0.23	0.58
PA/DNA	-0.07	0.45	-1.72	-0.74	-0.04	0.78	1.75	-0.80	0.34
Slide, Å									
DNA	0.78	2.87	0.80	0.29	-0.10	0.29	0.80	2.87	0.78
PA/DNA	-0.12	0.86	0.26	-0.15	0.90	-0.21	0.28	1.29	0.13
Rise, Å									
DNA	3.28	3.29	3.10	3.29	3.66	3.29	3.10	3.29	3.28
PA/DNA	3.28	3.16	3.39	3.20	3.28	3.24	3.33	3.06	3.19
Tilt, °									
DNA	3.32	-1.37	-3.91	2.23	0.00	-2.22	3.90	1.37	-3.33
PA/DNA	5.81	0.74	-8.44	0.18	-0.16	0.40	7.94	0.64	-5.68
Roll, °									
DNA	9.03	-7.95	9.87	-0.74	3.26	-0.74	9.89	-7.96	9.03
PA/DNA	7.70	8.79	11.19	2.85	7.23	2.47	10.59	9.57	3.58
Twist, °									
DNA	28.26	50.50	21.04	35.80	48.48	35.80	21.04	50.49	28.26
PA/DNA	33.68	30.23	35.16	32.13	35.93	32.04	35.32	29.68	32.64

*Relationship between the bases composing the base pair.
‡DNA corresponds to 0.73 Å structure of duplex DNA solved by Rees and coworkers (PDB 1D8G, 5'-CCAGTACTGG-3').

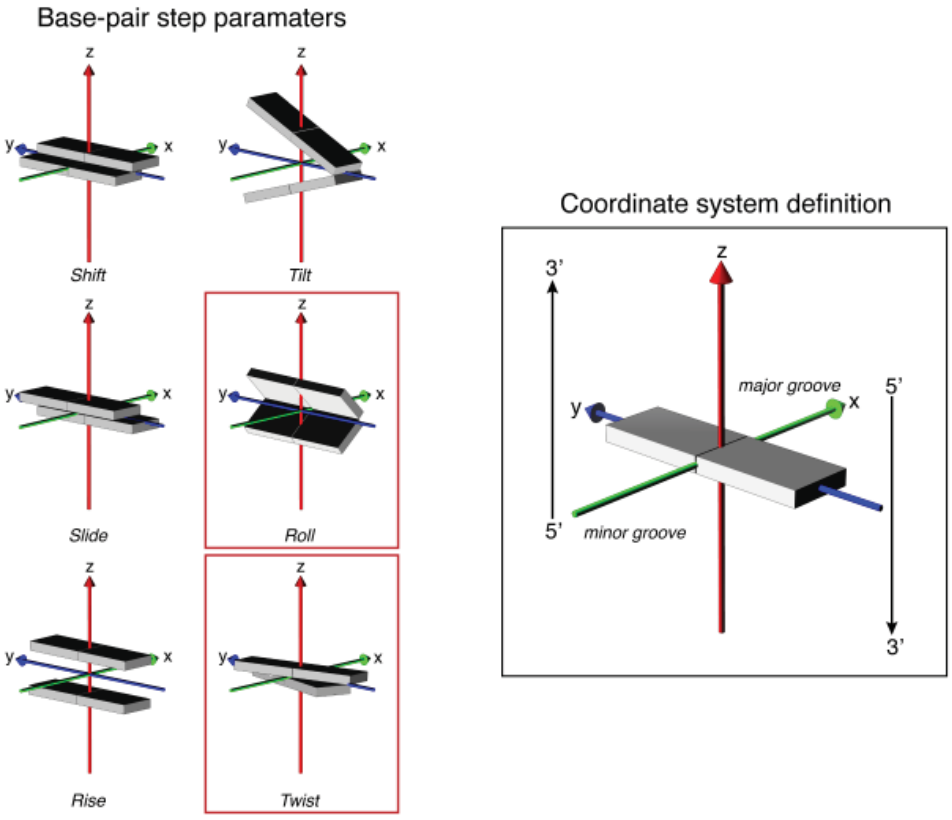

Figure 6.6 Comparison of Local base-pair step parameters for DNA with and without polyamide complexed. Parameters were calculated using 3DNA.

Local base-pair parameters and sugar pucker

Parameter*	C•G	C•G	A•T	G•C	T•A	A•T	C•G	T•A	G•C	G•C
Shear, Å										
DNA	0.15	0.32	0.02	-0.19	-0.09	0.09	0.19	-0.02	-0.32	-0.15
PA/DNA	0.15	0.19	0.13	-0.12	-0.13	0.13	0.12	-0.10	-0.16	-0.16
Stretch, Å										
DNA	-0.15	-0.16	-0.11	-0.07	-0.03	-0.03	-0.07	-0.11	-0.16	-0.15
PA/DNA	-0.14	-0.10	-0.11	-0.07	-0.10	-0.09	-0.10	-0.13	-0.04	-0.10
Stagger, Å										
DNA	0.09	0.12	0.08	0.25	0.00	0.00	0.25	0.08	0.12	0.09
PA/DNA	0.27	-0.02	-0.10	0.09	-0.02	0.04	0.09	-0.14	0.07	0.61
Buckle, °										
DNA	-6.41	-0.43	-1.63	10.75	13.15	-13.15	-10.74	1.63	0.44	6.42
PA/DNA	-10.59	-7.08	6.15	-2.23	0.37	1.17	2.39	-2.93	16.58	23.00
Propeller, °										
DNA	-15.16	-11.87	-3.23	-5.12	-10.90	-10.90	-5.15	-3.23	-11.87	-15.15
PA/DNA	-16.87	-6.31	-10.92	-4.05	-14.69	-16.26	-4.66	-7.96	-5.00	-17.05
Opening, °										
DNA	0.99	-1.15	1.35	1.26	-0.27	-0.27	1.27	1.34	-1.13	1.00
PA/DNA	0.68	1.71	3.84	-0.78	-4.87	-4.88	-1.10	3.78	0.87	-0.15
Sugar pucker										
DNA	O4'-endo C1'-exo	C2'-endo C3'-exo	C2'-endo C2'-endo	C1'-exo O4'-endo	C2'-endo C2'-endo	C2'-endo C2'-endo	O4'-endo C1'-exo	C2'-endo C2'-endo	C3'-exo C2'-endo	C1'-exo O4'-endo
PA/DNA	C3'-endo C2'-endo	C1'-exo C2'-endo	C2'-endo O4'-endo	C2'-endo C1'-exo	O4'-endo C1'-exo	C1'-exo O4'-endo	C1'-exo C2'-endo	O4'-endo C2'-endo	C2'-endo C2'-endo	C1'-exo C3'-endo

*Relationship between the bases composing the base pair.
‡DNA corresponds to 0.73 Å structure of duplex DNA solved by Rees and coworkers (PDB 1D8G, 5'-CCAGTACTGG-3').

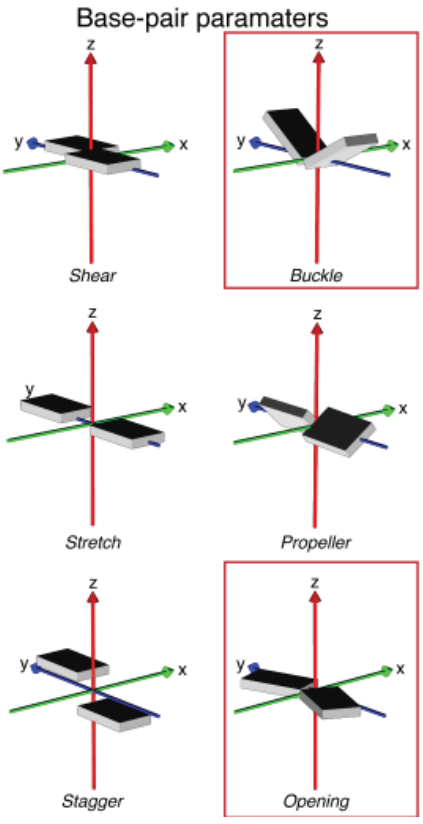

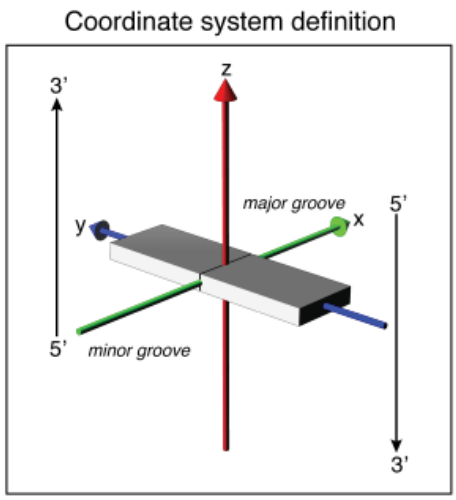

Figure 6.7 Comparison of Local base-pair parameters and sugar conformations for DNA with and without polyamide complexed. Parameters were calculated using 3DNA.

Local base-pair helical parameters

Parameter*	CC/GG	CA/TG	AG/CT	GT/AC	TA/TA	AC/GT	CT/AG	TG/CA	GG/CC
X-displacement, Å									
DNA	-0.42	3.84	-1.31	0.57	-0.41	0.57	-1.32	3.84	-0.42
PA/DNA	-1.36	-0.07	-1.21	-0.76	0.42	-0.81	-1.07	0.59	-0.34
Y-displacement, Å									
DNA	1.83	-0.36	-2.71	1.50	0.00	-1.50	2.71	0.36	-1.84
PA/DNA	0.98	-0.68	1.45	1.36	0.05	-1.34	-1.59	1.60	-1.52
Inclination, °									
DNA	17.85	-9.25	25.08	-1.20	3.96	-1.20	25.12	-9.26	17.85
PA/DNA	12.96	16.43	17.68	5.14	11.58	4.47	16.74	18.10	6.29
Tip, °									
DNA	-6.56	1.59	9.92	-3.62	0.00	3.60	-9.90	-1.59	6.59
PA/DNA	-9.78	-1.38	13.33	-0.33	0.26	-0.73	-12.56	-1.20	9.97

*Relationship between the bases composing the base pair.
‡DNA corresponds to 0.73 Å structure of duplex DNA solved by Rees and coworkers (PDB 1D8G, 5'-CCAGTACTGG-3').

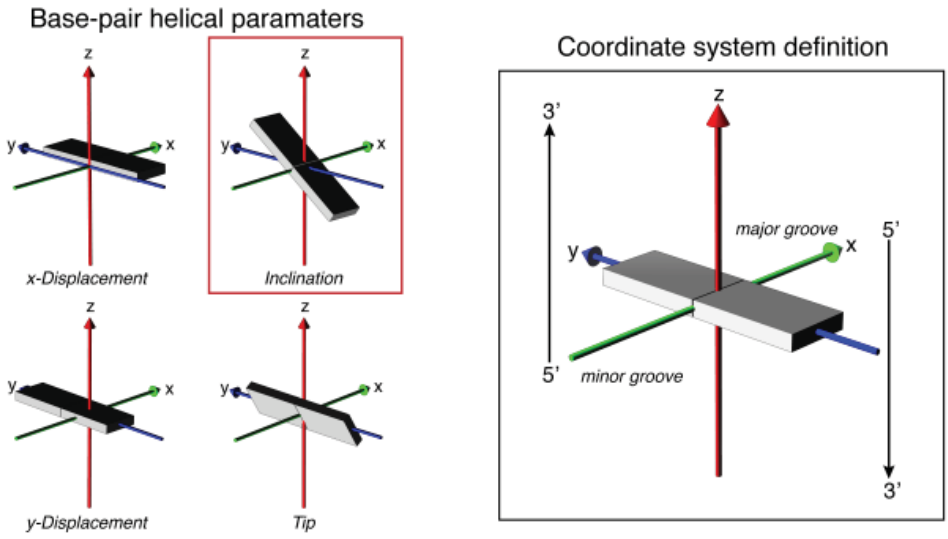

Figure 6.8 Comparison of Local base-pair helical parameters for DNA with and without polyamide complexed. Parameters were calculated using 3DNA.